Micro-milling of Selective Laser Melted Stainless Steel

Andrea Abeni, Paola Serena Ginestra, and Aldo Attanasio

Abstract This paper deals with micro mechanical machining process of 17-4 PH stainless steel samples fabricated by selective laser melting. An analysis of the material removal behaviour during micro-milling operations for the selection of the optimal feed rate value was performed on 17-4 PH additive manufactured samples studying the variation of the specific cutting force as a function of the feed per tooth. The transition from shearing to ploughing regime was analysed by considering the variation of the specific cutting forces. The minimum uncut chip thickness was calculated to identify the transition between the cutting regimes (shearing, ploughing or their combination) that affects the final product quality in terms of surface integrity and dimensional accuracy. Moreover, the surface roughness and the burr extension were analysed as a function of the feed rate.

Keywords Selective laser melting · Micro machining · Minimum uncut chip thickness

1 Introduction

Differently from conventional machining processes, Additive Manufacturing (AM) processes produce parts with complex shape by material addition. Depending on the material charging method, the AM techniques of metals can be classified in: powder bed fusion, direct energy deposition and wire fed systems. Selective Laser Melting

A. Abeni (✉) · P. S. Ginestra · A. Attanasio
Department of Mechanical and Industrial Engineering, University of Brescia, 25123 Brescia, BS, Italy
e-mail: andrea.abeni@unibs.it

P. S. Ginestra
e-mail: paola.ginestra@unibs.it

A. Attanasio
e-mail: aldo.attanasio@unibs.it

E. Ceretti and T. Tolio (eds.), *Selected Topics in Manufacturing*,
Lecture Notes in Mechanical Engineering,
https://doi.org/10.1007/978-3-030-57729-2_1

(SLM) is the most promising powder bed fusion process where a product is obtained by the selective melting of metal powders by a laser source. SLM allows the fabrication of products characterized by high structural integrity. On the other hand, the surface finish is inadequate and with high variability that in some cases can affect the technical properties and compromise the required tolerances [1]. The final properties of SLM metals are still under study due to the presence of uncontrolled porosities, defects and poor surface finishing states [2]. The poor surface quality of the SLM components resulting from a high surface roughness is mostly due to the partially melted powder on the outer surface of the manufactured parts collected during the building process [3]. Post processing is therefore needed for an improvement of the surface finishing and mechanical properties of the final parts.

Among the traditional processes used to achieve high precision on 3D components, micro milling is one of the most convenient micro manufacturing processes in terms of volume and cost ratio [4, 5]. Micro milling can be utilized to mechanically remove materials using micro tools to obtain complex micro-size features on a wide variety of engineering materials. However, the efficiency of micro milling introduces critical issues due to the miniaturization of parts and tools that requires a deep understanding and optimization of the process. Micro machining operations are characterized by a chip thickness comparable in size to the cutting edge radius of the mill. The increases in cutting energy and forces as the undeformed chip thickness decrease is one of the most significant size effects of micro milling. In particular, when the uncut chip thickness is lower than a minimum value (i.e. minimum uncut chip thickness), the cutting process is characterized by an elasto-plastic deformation of the material known as ploughing. This cutting regime is does not correspond to a correct chip formation. Thus, the Minimum Uncut Chip Thickness (MUCT) has been identified as the undeformed chip thickness at which the transition from ploughing to shearing occurs causing a significant variation of the normalized cutting energy and forces [6]. In order to increase productivity and improve the machined part quality during micro milling, the ploughing mechanism has to be understood. Moreover, the ploughing process has a direct impact on the final surface roughness of the treated material influencing the achievable accuracy of the finished AM components. Furthermore, the analysis of the dominant deformation regime during micro milling operations involves the cutting force measurement. The effects of the tool run-out must be considered to quantify the loads imbalance on the tool flutes during the process [7].

The objective of this paper is to study the material removal behaviour of 17-4 PH stainless steel parts produced by SLM and post processed by micro milling. The proposed analysis is based on the realization of microchannels with 800 μm width by using coated tungsten carbide micro end mills on SLM steel samples. The cutting force was acquired at a high sampling rate in order to avoid any aliasing effects. In particular, the cutting force has been analysed as a function of the feed per tooth in order to identify the occurring transition from ploughing to shearing. A proper analytical model to take into account the tool run-out effects while calculating the specific cutting forces was applied.

Moreover, the roughness (Ra) and the burrs dimension of the microchannel were analysed to relate the surface finishing to the material deformation mechanism during the process.

2 Experimental Procedure

In this section, the production and machining operations of the SLM 17-4 PH stainless steel samples are reported. The manufacturing parameters and the experimental plan followed for the micro milling tests are defined and the model used for the evaluation of the specific cutting force in presence of the tool run out is described.

2.1 Sample Production

The SLM samples were produced using the laser based powder bed fusion machine ProX 100 (3D System). The geometry of the samples was designed to allow the positioning of the samples on the load cell Kistler© 9317C. The samples were printed as squares with a side equal to 25 mm and a thickness equal to 5 mm with four holes with a diameter of 4.20 mm on the corners of the squares.

The chemical composition of the 17-4 PH stainless steel powder used as printing material is reported in Table 1.

The absence of impurities is necessary to avoid negative effects of embrittlement. Therefore, the laser process is carried out in a Nitrogen atmosphere with a controlled O_2 content less than 0.1 vol.%. The optimized parameters for the SLM of 17-4 PH steel of the process are reported in Table 2.

The as built samples were subjected directly to the micromachining tests without heat treatment.

Table 1 Chemical composition of 17-4 PH stainless steel powder

17-4 PH	C	Cr	Ni	Cu	Mn	Mo	Nb	Si
Wt (%)	<0.07	16.71	4.09	4.18	0.8	0.19	0.23	0.53

Table 2 Process parameters used in the SLM process

Process parameter	Value
Laser power (W)	50
Spot diameter (μm)	80
Scan speed (mm/s)	300
Hatch spacing (μm)	50
Layer thickness (μm)	30

2.2 Micro-milling Tests

The machining tests were carried out fabricating twenty channels by using a constant cutting speed and twenty different feed per tooth (f_z) values. Once the cutting forces were acquired and normalized, the ploughing-shearing transition was determined through the MUCT quantification. Moreover, the roughness and the burrs were measured and the data were evaluated as a function of the parameter f_z.

The cutting tests were performed on a five axis Nano Precision Machining Centre KERN Pyramid Nano equipped with a Heidenhain iTCN 530 numeric control. The loads generated by the interaction between tool and workpiece were measured through a force acquisition system, as reported in [8]. The precision of the load cell, the bandwidth and the sampling rate of the measurement system are adequate for capturing forces in micro milling [9]. The samples were constrained to the load cell through four bolts. The load cell was blocked to the machine work table. The experimental procedure consisted in two different milling operations: (i) a roughing to prepare a planar surface on the workpiece and (ii) micro slot machining, executed varying the *fz* at each test. The force acquisition was performed during the micro slot machining. The roughing was performed through four identical consecutive passes with a depth of cut of 100 μm for each step. A four-flutes flat-bottom mill with a nominal diameter of 6 mm was employed to prepare the samples setting a cutting speed equal to 40 m/min and a feed per tooth of 10 μm/tooth. The microchannels were produced using a coated two flutes micro mill with a nominal diameter of 0.8 mm. The actual tool geometry was acquired using a confocal microscope (Hirox RH 2000). Further tool information are reported in Table 3.

The tests were designed with the purpose of identifying the MUCT as a function of the feed per tooth. On each side of the 17-4 PH stainless steel workpiece, five cuts were performed moving the tool from the outer to the centre at a constant depth (a_p) of 200 μm. A cutting speed (v_c) of 40 m/min was kept constant for each cut. An actual tool diameter of 789 μm was measured by means of the BLUM laser measuring system mounted on the CNC machine.

Figure 1 illustrates the machining pattern and the load cell reference systems that was aligned to the KERN machine tool. Twenty micro channels were machined by

Table 3 Process parameters used in the micromilling process

Properties	Value
Nominal (μm)	800
Effective diameter (μm)	789 ± 2
Nominal cutting edge radius (μm)	5
Effective cutting edge radius (μm)	6.3
Helix angle (°)	20
Rake angle (°)	4
Material	Tungsten carbide
Material coating	Titanium nitride

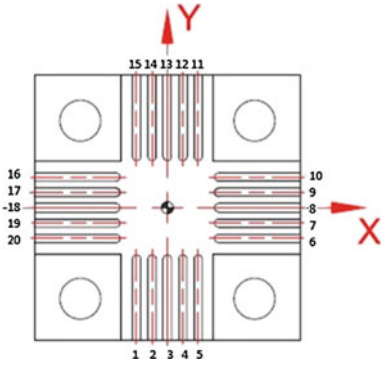

Fig. 1 Micro-slot pattern with the related reference systems

using twenty feed per tooth values ranging between 10 and 0.5 μm. The tool wear has been measured with a digital optical microscope and resulted negligible. Between two consecutive tests the tool has been properly cleaned to remove any stick material as confirmed by the optical microscope observations.

The force acquisition system allows to measure the cutting load component along each direction. The single components were subsequently composed to calculate the cutting force (F_c) through Eq. (1) directly in LabVIEW, the integrated development environment for the National Instruments graphic programming code.

$$F_C = \sqrt{(F_X)^2 + (F_Y)^2 + (F_Z)^2} \tag{1}$$

LabVIEW code was integrated by a Butterworth 20th order low-pass filter with a cut-off frequency of 1000 Hz. The tooth pass frequency corresponding to cutting speed and the tool can be calculated by Eq. (2).

$$f_{TP} = \frac{n}{60} * z \tag{2}$$

Considering the number of tool flutes ($z = 2$) and the spindle speed (n = 15,923 rpm), the tooth pass frequency is equal to 530 Hz and consequently it is lower than the cut-off frequency. The signal was filtered in order to identify the cutting force maximum peak on the flutes for each rotation. As shown in Fig. 2, the maximum peaks of the signal were not substantially altered.

2.3 Evaluation of the Normalized Specific Force Fc

The experiments allowed to investigate the regime transition as a function of the process f_z. The cutting force can not be directly used in this analysis and it must be normalized regarding the chip cross-section (S). Equation (3) shows the relation between chip section and feed per tooth:

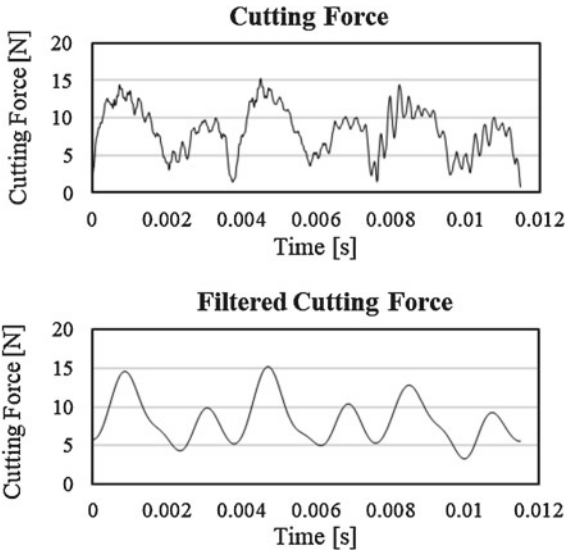

Fig. 2 Comparison between the original cutting force and the filtered cutting force

$$S = a_p * h \tag{3}$$

where a_p is the axial depth of cut while the chip thickness h can be calculated by Eq. (4)

$$h = f_z * \sin(\omega t) \tag{4}$$

In particular, the maximum cross section ($\omega t = \pi/2$) is expressed by the product between the axial depth of cut (a_p) and the feed per tooth (fz). The decrease of fz between two consecutive test determines a section (S) reduction which has a considerable effect on the cutting force value. To highlight the dependence of the cutting force in relation to the deformation mechanism, a specific cutting force must be calculated by Eq. (5):

$$F_{cn} = \frac{Fc}{S} \tag{5}$$

where Fc is the cutting force results from the combination of all the force components including the cutting edge component. The specific force allows to identify the MUCT. During ploughing regime, the workpiece material elasto-plastic deformation determines a load increment. The phenomenon is enhanced by the accumulation of uncut material against the cutting edge. When shearing regime is prevalent, the correct chip formation causes the specific loads decrease. A direct correlation between the regime transition and the specific cutting force must be identified without neglect the tool run-out effects. The tool run-out causes a difference between the effective

chip thicknesses on each flute, determining an unbalanced load condition on the flutes. Considering two flutes, the maximum chip thickness for one flute (h_{Amax}) will be greater than the thickness for the other flute (h_{Bmax}). The asymmetric condition causes two cutting force peaks ($Fcmax_A$; $Fcmax_B$) which should be normalized by considering the effective thickness (see Fig. 2). Several tool run-out models should be utilized [8, 10, 11]. The simplest approach is based on the hypothesis of a direct relation between chip section and force peak. Equation (6) was implemented to calculate the effective chip thickness for tool flute A:

$$h_{Amax} = \frac{2 * Fcmax_A}{Fcmax_B + Fcmax_A} * f_z \quad h_{Bmax} = 2f_z - h_{Amax} \tag{6}$$

where $\frac{Fcmax_B + Fcmax_A}{2}$ is the average force peaks between edge A and edge B (Fc_{av}). Supposing that the average undeformed chip thickness is equal to f_z, Eq. (6) derived from the proportion $h_{Amax} : Fcmax_A = Fc_{av} : f_z$. The signal of the Fc was considered in order to select a uniform portion corresponding to thirty tool rotations. For each spindle rotation the effective chip thickness h_{Amax} was calculated and subsequently an average value was obtained. The average value was finally utilized for the force normalization.

2.4 Roughness and Burrs Evaluation

The roughness was evaluated by means of a Mitutoyo SJ300 profilometer with a 2 μm tip. The width (W_B) and height (H_B) of each burr were measured for each inner and outer channel side. The burrs width was measured by using a Mitutoyo QuickScope optical coordinate measuring machine, while the burrs height was measured by using a Hirox RH-2000 optical microscope (Fig. 3).

The width and the height were combined supposing the absence of curvatures of the burrs to obtain a unique value of the length (L_B) of the burrs on each side

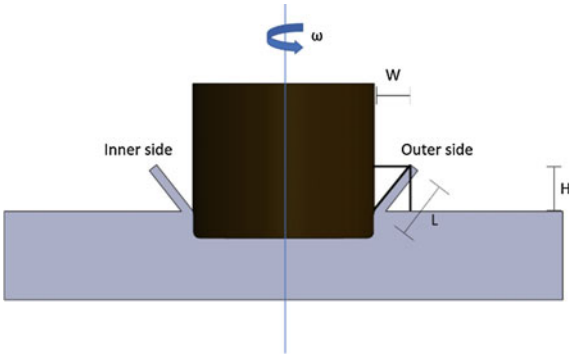

Fig. 3 Schematic representation of the geometry of the burrs

according to Eq. (7):

$$L_B = \sqrt{(W_B)^2 + (H_B)^2} \tag{7}$$

The collected data were reported as function of the feed per tooth in order to evaluate the dependence of roughness and burrs in relation to the feed rate.

3 Results and Discussion

In this section, the results related to the evaluation of the transition regime of deformation are reported. Tables 4 and 5 reports the values of the average specific cutting forces (Fc_n) calculated considering both the actual depth of cut (a_{peff}) and the force peaks ($Fcmax_A$, $Fcmax_B$).

Figure 4 shows the measured cutting force peaks for each flute. The difference between the force peaks can be related to the tool run-out. It is possible to observe that when the feed per tooth is higher than 2 μm, the tool run-out influence slightly increases as the feed per tooth decreases. In fact, it is evident that the difference between the force peak of the flute A and the force peak of the flute B increases as the feed rate decreases. When the feed per tooth is equal or lower than 2 μm, the difference between the cutting force peaks strongly increases as the feed per tooth decreases. This behaviour can be related to a ploughing condition involving flute B that causes an increment of the undeformed depth of cut for flute A. Consequently, the normalization performed on the resulting cutting force values allowed to investigate the cutting regime of the AM material by making the tool run out effects negligible.

Observing Fig. 5, the specific cutting force is not constant thorough the tests due to the presence of different deformation mechanisms. It shows an increase of the

Table 4 Results of the micromilling tests performed at different feed per tooth values ranging between 5.5 and 10 μm/tooth * rev

n	f_z (μm/t)	a_{peff} (μm)	$Fcmax_A$ (N)	$Fcmax_B$ (N)	Fc_n (N/mm^2)
1	10	205.4	18.7	14.1	8016.0
2	9.5	205.7	14.0	9.9	6127.6
3	9	201.3	13.2	9.1	6177.5
4	8.5	203.1	15.1	10.0	7266.7
5	8	203.3	10.4	8.6	5887.3
6	7.5	199.9	12.5	4.2	5595.4
7	7	198.1	11.0	1.9	4684.5
8	6.5	198.3	11.1	2.4	5251.8
9	6	200.7	11.4	2.5	5840.3
10	5.5	203.4	13.0	4.5	7857.1

Table 5 Results of the micromilling tests performed at different feed per tooth values ranging between 0.5 and 5 μm/tooth * rev

n	f_z (μm/t)	a_{peff} (μm)	$Fcmax_A$ (N)	$Fcmax_B$ (N)	Fc_n (N/mm^2)
11	5	200.5	12.2	4.1	8175.1
12	4.5	199.3	10.5	3.6	7960.0
13	4	198.9	11.7	2.5	9007.8
14	3.5	199.1	11.0	2.1	9515.1
15	3	198.7	10.9	2.1	10,994.4
16	2.5	209.8	10.6	1.6	11,766.8
17	2	206.3	15.2	3.1	22,277.7
18	1.5	200.8	15.6	4.3	33,253.7
19	1	205.8	17.3	3.0	49,514.9
20	0.5	202.6	17.8	1.9	97,726.5

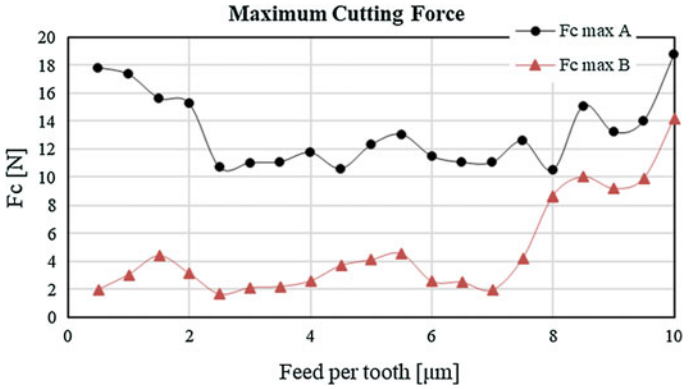

Fig. 4 The maximum cutting force value for each flute versus feed per tooth

normalized cutting force when the feed per tooth decreases from 2.5 to 2 μm/tooth. This trend allows to set the MUCT value to 2.5 μm/tooth. Considering the deformation mechanisms, region I corresponds to a ploughing dominated regime extended to a feed per tooth value of 2.5 μm/tooth according to literature [6], which identifies the MUCT value as the 20–40% of the cutting edge radius. The identified MUCT value is also in accordance with the behaviour observed in Fig. 4. On the other hand, region III is related to the shearing deformation regime characterized by an independence of the specific cutting forces from the feed per tooth values, as visible from the reported magnification of the specific cutting force. The region II can be identified as a transition zone between the two dominant deformations mechanism where the ploughing effects are progressively increasing as the feed per tooth decreases.

The roughness of the as built SLM parts was measured on three replica of the same samples and resulted in 12.85 ± 0.18 μm. The micro machining tests significantly

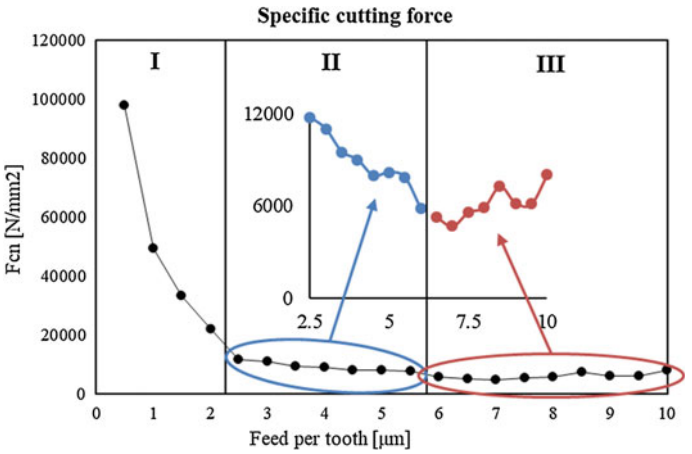

Fig. 5 Specific cutting forces versus feed per tooth

improved the surface quality as required by standard mechanical application. The effects of the occurring of the ploughing regime are visible on the evaluation of the roughness trend reported in Fig. 6.

As shown, high average roughness values are also related to the higher sensitivity to run out of the kinematic roughness at lower values of f_z. Moreover, the increased variability of the results is probably due to the incorrect chip formation mechanism during ploughing that is responsible of uncontrollable irregularities and accumulation of material thought the flute path. On the other hand, when the shearing regime is dominant, the mean roughness values depend on the feed per tooth values according to the typical trend of cutting tests. Moreover, the reduced variability of the data demonstrates the transition to a more regular deformation mechanism.

The burr length was considered to evaluate the influence of the ploughing regime on the feature quality (Fig. 7).

Fig. 6 Average roughness versus feed per tooth

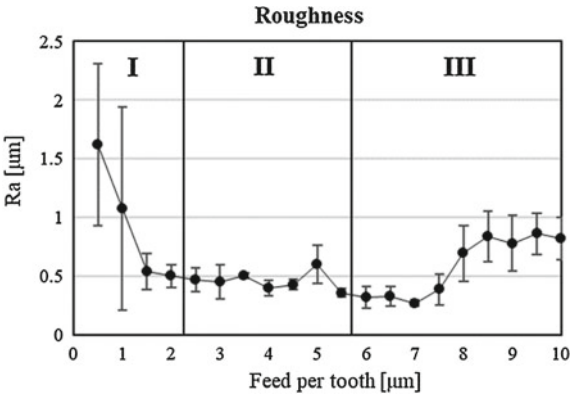

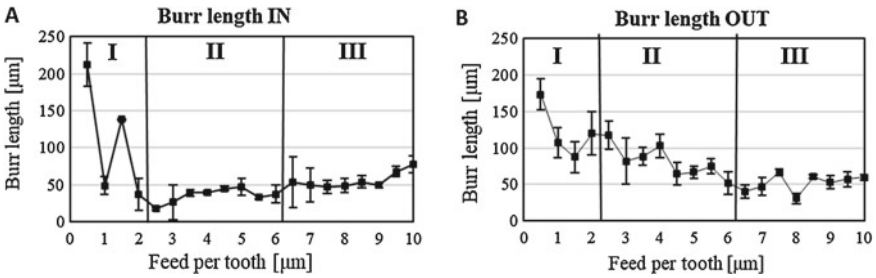

Fig. 7 Burr length on the inner side (**a**) and burr length on the outer side (**b**) versus feed per tooth

As expected, the length of the burrs on the outer side is higher compared to the length on the inner side.

The burr length on the inner side of the channels is strongly influenced by the occurring of the ploughing regime as highlighted from an increase of the average values. As the shearing regime is dominant, the length of the burrs begins to be dependent on the feed rate as visible from the trend of the data. On the other hand, the burr length on the outer side is more variable probably due to the instability of the ploughing regime and the presence of compressed AM material.

4 Conclusion

In this paper, the material removal behaviour of additive manufactured stainless steel was analysed. The specific cutting force resulting from the production of microchannels on SLM samples was evaluated as a function of the feed per tooth to identify the transition of the material from ploughing to shearing deformation regime. Moreover, the roughness and the burrs dimension of the machined workpiece were measured to investigate the effects of the deformation mechanism on the surface final finishing.

From the results it is possible to notice a ploughing dominated regime at low feed per tooth values followed by a transition to a shearing dominated regime at higher feed rates. In particular, the specific cutting forces related to the ploughing regime resulted ten times higher than the forces calculated when shearing regime is present. As expected, at the highest feed per tooth values the specific cutting force was found to be independent on the feed rate value. The results showed a behaviour transition of the material at the 30–35% of the effective tool edge radius. Thus, the study allowed to identify an optimal feed per tooth range related to reduced cutting forces with the aim of minimize the tool damage probability and consequently the tool wear rates.

Furthermore, the highest values of roughness were measured on the surface of the channels machined at low feed rates. The variability of the data showed a progressive decrease corresponding to a more dominant shearing regime. The dimension of the burrs calculated both on the inner and outer channel sides resulted higher at low feed per tooth values. Therefore, a high value of the feed rate is recommended to

reduce the extension of the burrs and assure a correct mechanical coupling between the micro-sizes components.

A further development of this research will be based on the comparison between the additive manufactured and the conventionally produced components under machining operations.

References

1. Leary M (2017) Surface roughness optimisation for selective laser melting (SLM): accommodating relevant and irrelevant surfaces. In: Brandt M (ed) Laser additive manufacturing. Woodhead Publishing Series in Electronic and Optical Materials, pp 99–118
2. Galy C, Le Guen E, Lacoste E, Arvieu C (2018) Main defects observed in aluminum alloy parts produced by SLM: from causes to consequences. Addit Manuf 22:165–175
3. Kaynak Y, Tascioglu E (2018) Finishing machining-induced surface roughness, microhardness and XRD analysis of selective laser melted Inconel 718 alloy. Procedia CIRP 71:500–504
4. Camara MA, Rubio C, Abrao AM, Davim JP (2012) State of the art on micromilling of materials, a review. J Mater Sci Technol 28:673–685
5. Malekian M, Park S, Jun MBG (2009) Modeling of dynamic micro-milling cutting forces. Int J Mach Tools Manuf 49:586–598
6. Malekian M, Mostofa MG, Park SS, Jun MBG (2012) Modeling of minimum uncut chip thickness in micro machining of aluminum. J Mater Process Technol 212:553–559
7. Attanasio A (2017) Tool run-out measurement in micro milling. Micromachines 8:221
8. Attanasio A, Abeni A, Özel T, Ceretti E (2019) Finite element simulation of high speed micro milling in the presence of tool run-out with experimental validations. Int J Adv Manuf Technol 100(1–4):25–35
9. Attanasio A, Garbellini A, Ceretti E (2015) Force modelling in micromilling of channels. Int J Nano Manuf 11(5–6):275–296
10. Jin X, Altintas Y (2012) Prediction of micro-milling forces with finite element method. J Mater Process Technol 212:542–552
11. Zhang X, Ehmann KF, Yu T, Wang W (2016) Cutting forces in micro-end-milling processes. Int J Mach Tools Manuf 107:21–40